Tagger design optimization

M. Mazouz, J. Berger, J.F. Muraz, A. Patti, F. Vezzu, E. Voutier

Tagger Design Optimization

Malek Mazouz[1], Jacques Berger[1],
Jean-Francois Muraz[1], Adrien Patti[1] Francis Vezzu[1],
Eric Voutier[1,2]

[1] *Laboratoire de Physique Subatomique et de Cosmologie*
IN2P3-CNRS/Université Joseph Fourier
53 avenue des Martyrs
38026 Grenoble cedex, France

[2] *Thomas Jefferson National Accelerator Facility,*
12000 Jefferson avenue
Newport News, Virginia 23606, USA

Abstract

This note presents the simulations and tests performed at LPSC Grenoble for the optimization of the DVCS tagger paddles. The choice of the wrapping material and the addition of a light guide with a specific triangular cut are discussed and confronted to experimental measurements. This study led to the final configuration of the DVCS tagger.

Contents

1 Introduction

The DVCS tagger is used in the E03-106 experiment [1] to achieve the proton/neutron discrimination. It is composed of 57 scintillator paddles organized in two overlapping layers facing the Proton Array (Fig. 1). The specific design of each detector elements has been opitimized within the GEANT simulation package, considering the high background rates forseen in the DVCS experiment [2].

The purpose of this note is to present the procedure used to work-out an optimized configuration of the tagger paddles. Relying on simulations and experimental measurements, the signal shape end charcterisitics is studied and analyzed in the context of the uniformity of light collection.
The three next sections of this note present the prototype paddle and the experimental measurements made with the cosmics set-up installed in Grenoble. Then the evolution of the prototype configuration is discussed to obtain the final design of an elementary paddle of the DVCS tagger.

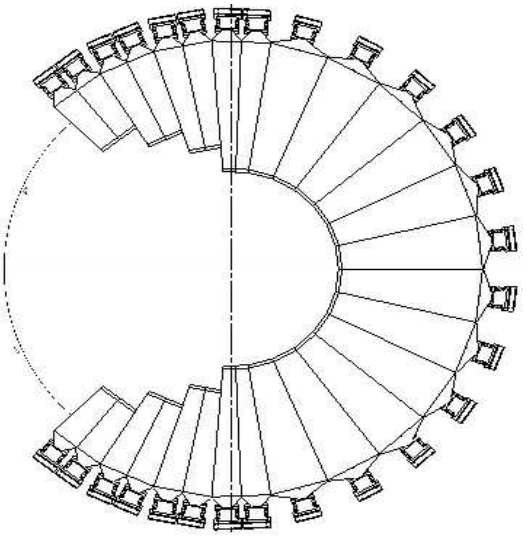

Figure 1. View of the second scintillator layer assembly.

2 Prototype detector

2.1 Paddle assembly

The response of scintillator paddles was experimentally investigated with two identical prototype paddles. The scintillator chosen was a 2 cm thick EJ200 procuced by the ELJEN company [3]. The ELJEN diamond-milled machining was carefully checked with respect to specifications given in Fig. 2. Each

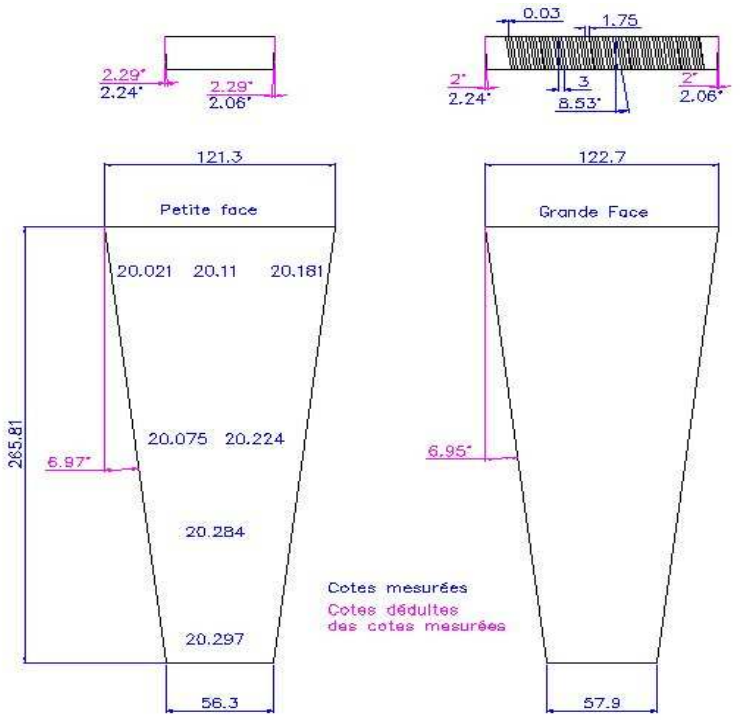

Figure 2. Geometrical characteristics of prototype paddles.

scintillator is surrounded by two wrapping layers: a first layer made out of aluminum or millipore for light reflexion purposes, a second layer constituting of black Tedlar for external light tightness. The paddles are read-out by a R7877 Hammamatsu Photomultiplier tube (PMT) which is fixed on the scintillator via a plastic housing (Fig. 3).

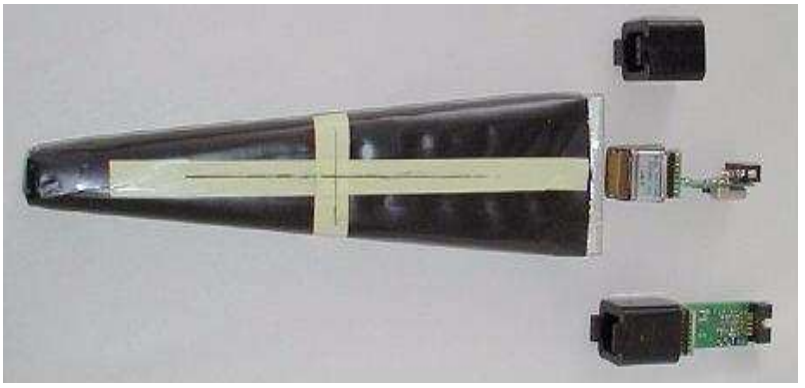

Figure 3. Tagger paddle assembly.

2.2 Electronics read-out

The signal issued from the PMT is supplied to an Analog Ring Sampler (ARS) which every 1 ns encodes the input over a time window of 128 ns. The output of the ARS module is then composed of 128 values which correspond to the

different amplitudes of the input signal as a function of time (Fig. 4). The output signal is characterized by several variables: the maximum amplitude, the full width at half of the maximum (FWHM), the rising time, etc... which are determined for each recorded signal from the 128 amplitude values set. Therefore, the maximal amplitude (called amplitude afterward) corresponds to the minimal value over the 128 samples (< 0) corrected for the ARS average baseline. This latter is determined from pedestal events and was shown to be stable within 3 mV all along the test period (Fig. 4).

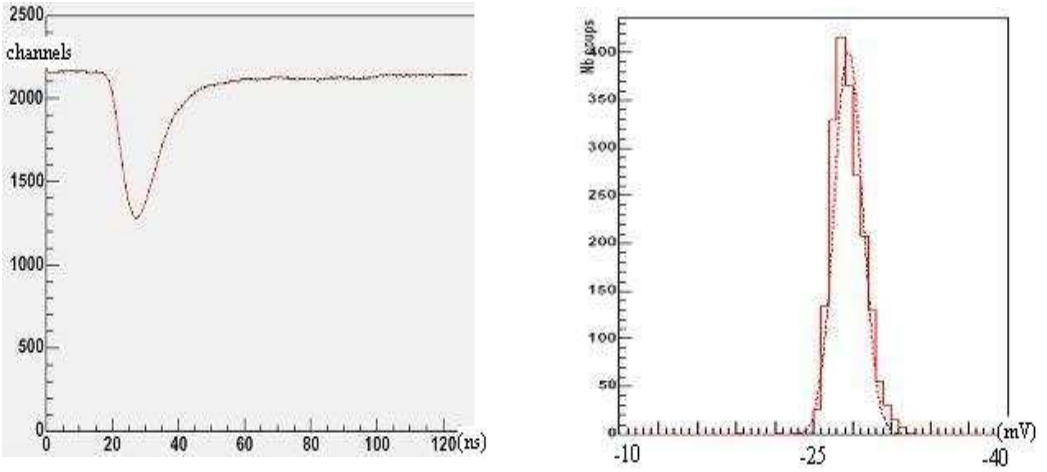

Figure 4. ARS signal characteristics: typical signal shape (left) and baseline histogram (right).

3 Cosmics set-up

The proton tagger (or veto) is composed of 57 paddles with 11 different shapes distributed in two layers. In the n-DVCS experiment, the tagger is used for the detection of 0.3-1 GeV/c protons which energy deposit in scintillators is 9-3 MeV/cm respectively. In abscence of any corresponding radioactive source, the prototype paddles are tested with cosmic muons. Using 70 cm lead (Fig. 5), we can select high energy particles. Energy deposit is 2 MeV/cm, close to the DVCS proton deposit.

High energy muons are selected via the coincidence between the S1 and S2 scintillator planes, the latter S2 is placed after the lead absorber. The scintillator coincidence is used to trig the acquisition system and to enable the read-out of the ARS information (Fig. 6). The prototype set-up, composed of the two prototype paddles (Fig. 5), is placed between three wire chambers that determine the coordinates of muon trajectories. The position of the impact point in the paddle plane is reconstructed with an accuracy about 2 mm. The limited surface of the scintillators defines a narrow solid angle which en-

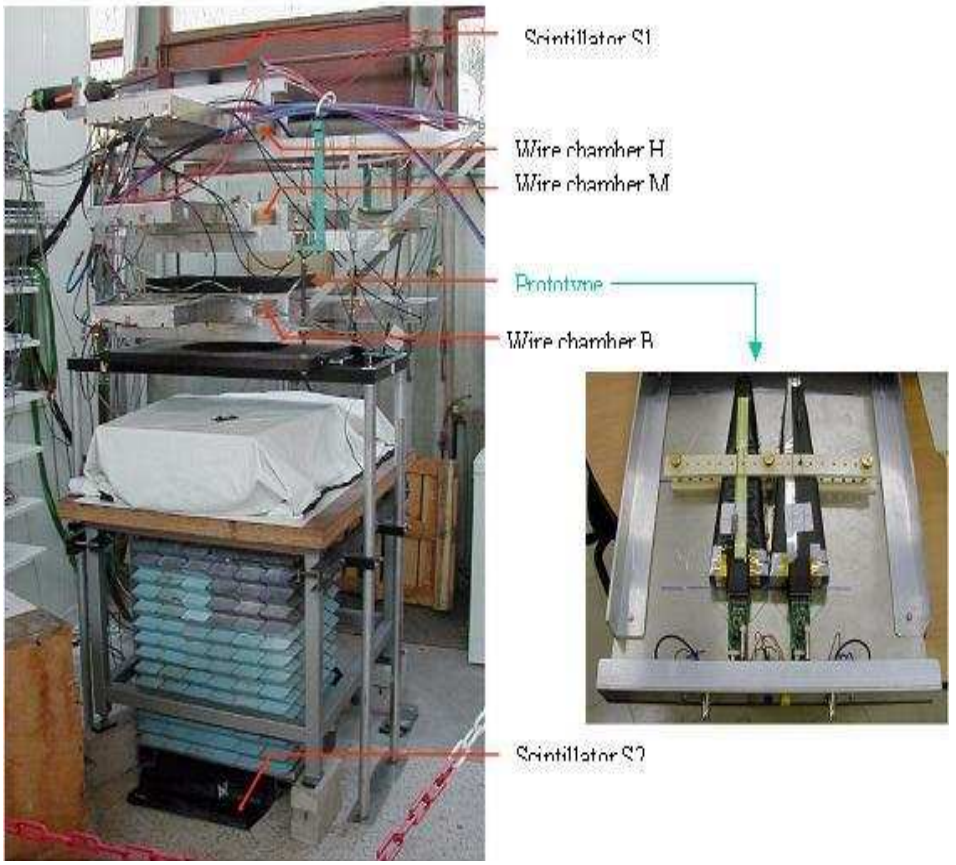

Figure 5. The cosmics experimental set-up.

sures a very small variation of the incident angle of muon trajectories in the prototype paddles, close to perpendicular.

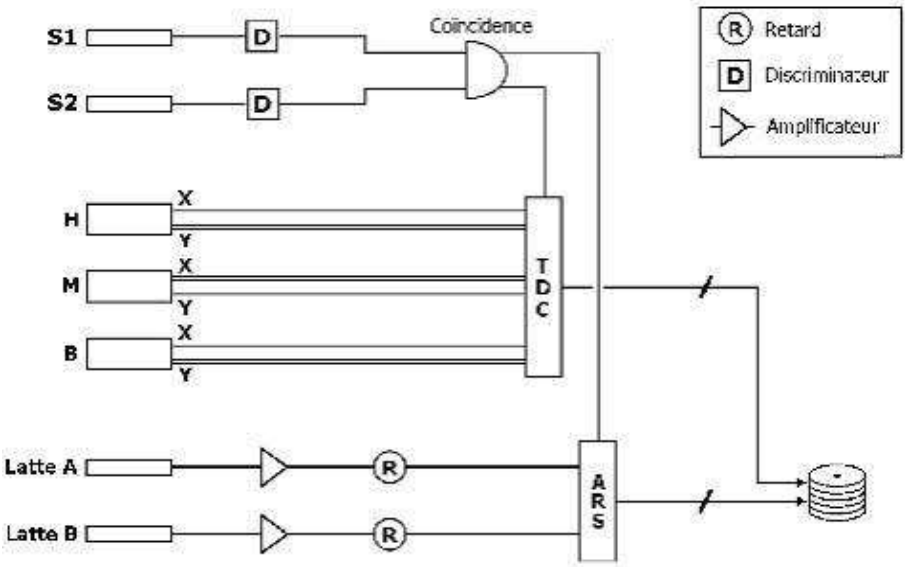

Figure 6. Synoptic of data acquisition.

4 Prototype testing

4.1 Signal characteristics

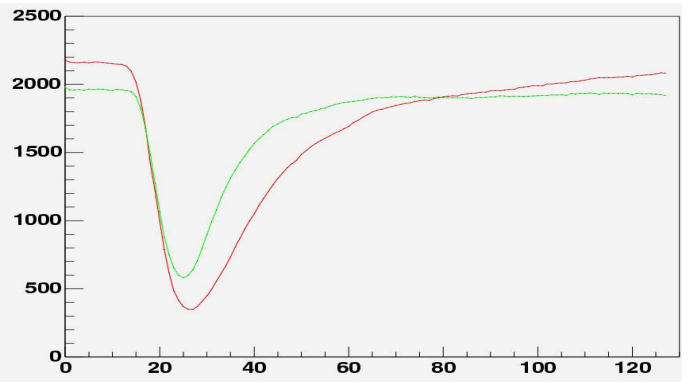

Figure 7. Two typical signals for the protype testing: aluminum wrapping (green), and millipore wrapping (red).

The prototype testing has been performed considering two different wrapping materials, aluminum (paddle A) and millipore (paddle B), Their optical properties should affect the light propagation in the scintillator. Two typical signals for this configuration are shown on Fig. 7. The main difference between them is the signal width.

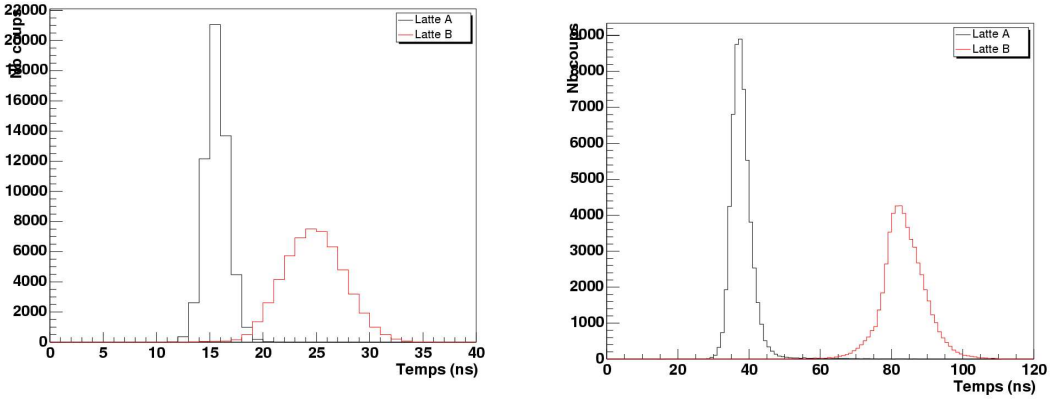

Figure 8. Full signal width: at 50% of the maximum (left) and at 10% of the maximum (right) (Latte A = aluminium, Latte B = millipore.

The two histograms of Fig. 8, representing the full width at 50% and at 10% of the maximum, show a widening of the signal in the case of a millipore wrapping. Aluminum behaves as a good light reflector and guides the emitted photons to the PMT with a small dispersion of their path length, leading to the observed width. On the other hand, the diffusive nature of millipore induces a larger range of light reflexion angles, increasing the photon path-length dispersion and therefore the signal width. This property also affects

the maximum amplitude of the signal which tends to be higher for millipore wrapping.

4.2 Amplitude distribution

The maximum amplitude of the signal is statistically distributed according to several phenomena: energy distribution of incoming muons, scintillation light law, photon propagation effects, PMT quantum efficiency... It is important to know wether the highest or the lowest amplitudes are correlated with certain regions of the paddle. The relative average amplitude allows to study the light collection uniformity as a function of the location of the muon track in the scintillator. The relative average amplitude for each cm^2 is defined by

$$A_{cm^2} = \sum_{i=1}^{n_{cm^2}} \frac{A^i_{cm^2}}{n_{cm^2}} \Big/ \sum_{i=1}^{n_{Tot}} \frac{A^i}{n_{Tot}} \tag{1}$$

where n_{cm^2} is the total number of events in the considered area, and n_{Tot} is the total number of events per paddle. This relative average amplitude is represented on Fig. 9 for the two prototype paddles; each colour corresponds to a given value of this variable, accessible from the scale. By definition, the average equals 1, and the fluctuation around this value tells about the uniformity of the light collection.

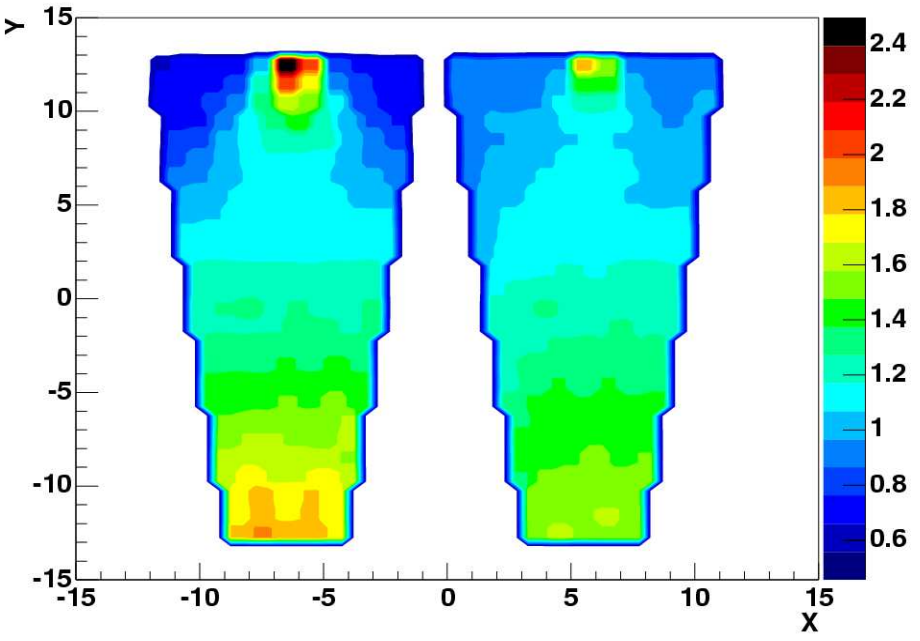

Figure 9. Light collection map of for the two prototype paddles: aluminum wrapping (left), and millipore wrapping (right).

In front of the PMT, the amplitude is quite above average (2.4 for paddle A, and 1.8 for paddle B), whereas the amplitude in the corner regions is below average (0.6 for paddle A, and 0.8 for paddle B). The higher amplitude originates from the larger PMT solid angle for emitted photon when close to the PMT entrance face, the lower ones resulting from a minimal direct view of the PMT. Also, the light collection uniformity is shown to be better in the case of a Millipore wrapping, as a consequence of the diffusive properties of this material.

Simulations reproduce the same dynamics of the light collection uniformity

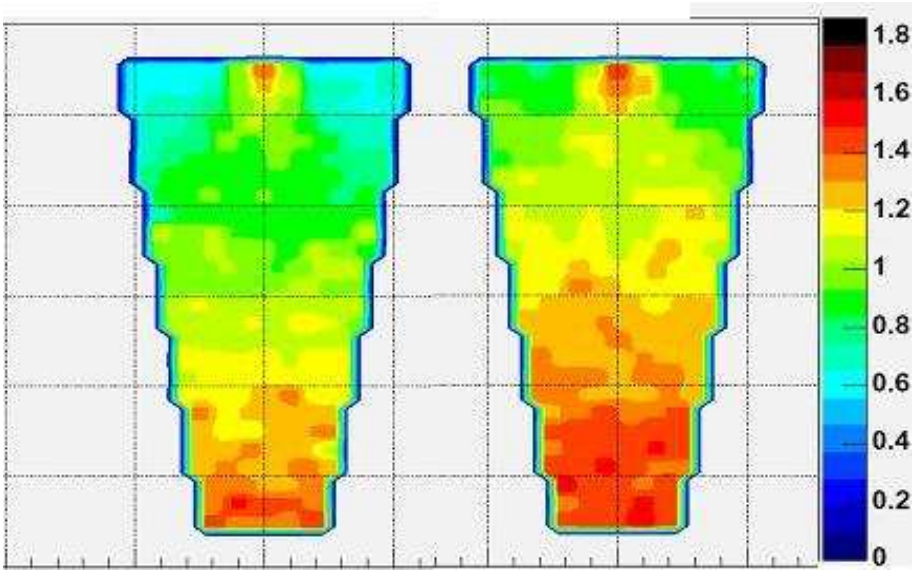

Figure 10. Simulated light collection maps: aluminum wrapping (left), and millipore wrapping (right).

but not the absolute amplitude values (Fig. 10). These are obtained using the LITRANI routine, developed by F.X. Gentit [4], which is a general simulation package for the propagation of optical photons The details of all simulations results are repoted in annex to this note..

To summarize, this test shows that aluminium wrapping is appropriate for low signals width, at the expense of a bad uniformity of the light collection. However, the signal width and duration are very important detection parameters. So aluminum wrapping was selected while investigating alternative light collection scheme to improve uniformity.

5 Tagger optimization

5.1 Phototube interface

The previous study of prototype paddles (Fig. 9) shows an increase of the relative average amplitude at the bottom part of the paddle. This effect does

not depend on the wrapping material and is confirmed by simulations (Fig. 10). Indeed, the absence of an optical connection between the scintillator and the PMT introduces a thin air layer between them and therefore an optical index change. Consequently, this layer reflects photons with large incident angle with respect to the PMT surface. Even if reflected once or twice, photons originating from the bottom part of the paddle have usually a normal incidence, due to the paddle particular geometry, contrary to other photons issued from a different region of the scintillator. Because normal incident photons are not reflected, this favors the light collection from the paddle bottom.
To reduce the importance of this effect, the thin air layer is replaced by an optical gel(Bicron BC630), having approximately the same index than the scintillator and the PMT surface. This cancels the optical index change effects and improves the light collection uniformity as seen on Fig. 11.

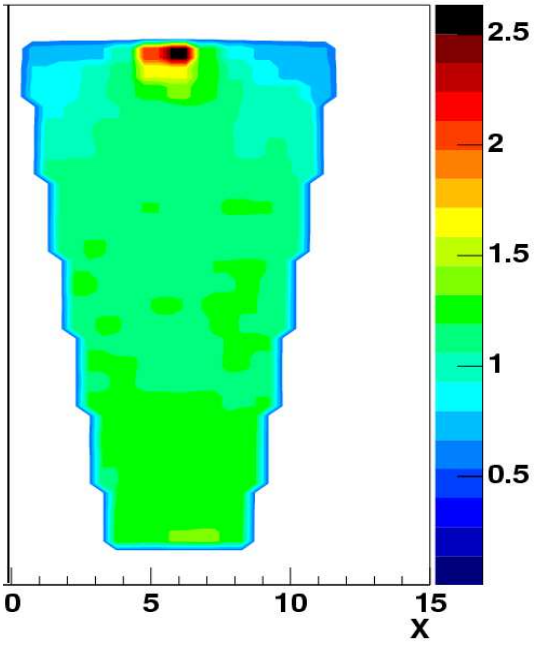

Figure 11. Light collection map using an optical gel and aluminum wrapping.

5.2 Light collection uniformity

The paddle configuration using aluminum wrapping and an optical gel still shows large variations of the relative average amplitude in the top part of the scintillator, close to the PMT entrance window (Fig. 11). This effect is a direct consequence of the acceptance (solid angle) of the PMT and can be minimized by increasing the distance between the scintillator and the PMT entrance, leading to the introduction of a light guide (Fig. 12).
This light guide was chosen to be PMMA plastic, easy to machine, having advantages of a high optical transmission and the absence of scintillation. This latter property reduces background sensitivity to the Čerenkov effect. The

optimization of the guide dimensions must comply with two specific requirements:

- a 8 mm high (at least) straigth part is needed to fix the PMT box;
- due to mechanical constraints, the light guide must not be higher than 3 cm.

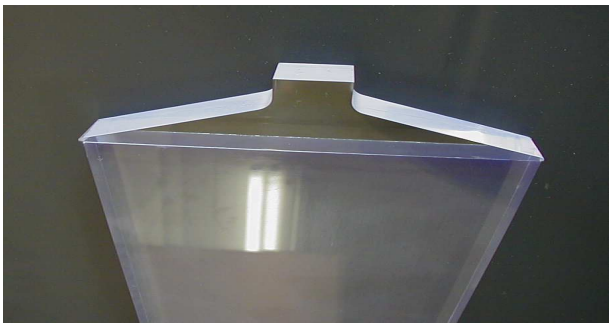

Figure 12. Light guide configuration.

Simulations have been worked out considering the total height of the guide and the height of the straight part as variable parameters. Results are reported on Tab. 1 [1] where the important parameter is ΔA, the difference between the extrema amplitudes. As expected, the larger the distance between the scintillator and the PMT (that is the total height of the guide) is, the better the uniformity of the light collection. More generally, simulations confirm that the light guide angle should be as large as possible.

Guide	$\mathbf{\Delta A}$	$\delta\mathbf{\Delta A}$	$\mathbf{A_{M}}_{in}$	$\mathbf{A_{M}}_{ax}$
1+0	0.56	0.06	0.72	1.28
1+1	1.18	0.07	0.55	1.73
2+0	0.33	0.07	0.82	1.15
2+1	0.35	0.02	0.78	1.13
3+0	0.31	0.02	0.82	1.13
3+1	0.25	0.02	0.85	1.10

Table 1. Optimization of the light guide dimensions, assuming a configuration with aluminum wrapping and optical gel: 2+1 means that the guide is 3 cm total high with a 1 cm straight part.

Considering the mechanical constraints on the tagger, the 2+1 light guide (3 cm guide height with a 1 cm straight part) seems to be the best solution for the light collection uniformity. The simulated light collection map shown on Fig. 13 with and without light guide, clearly shows the advantages of the light guide.

[1] A larger set of simulations was done for optimization purposes (different guide material, different shapes,...) and is reported in annex to this note; a typical short cut is given here.

This optimization procedure was achieved for every different paddle shape, and the 2+1 light guide was selected for each paddle (simulation results reported in annex).

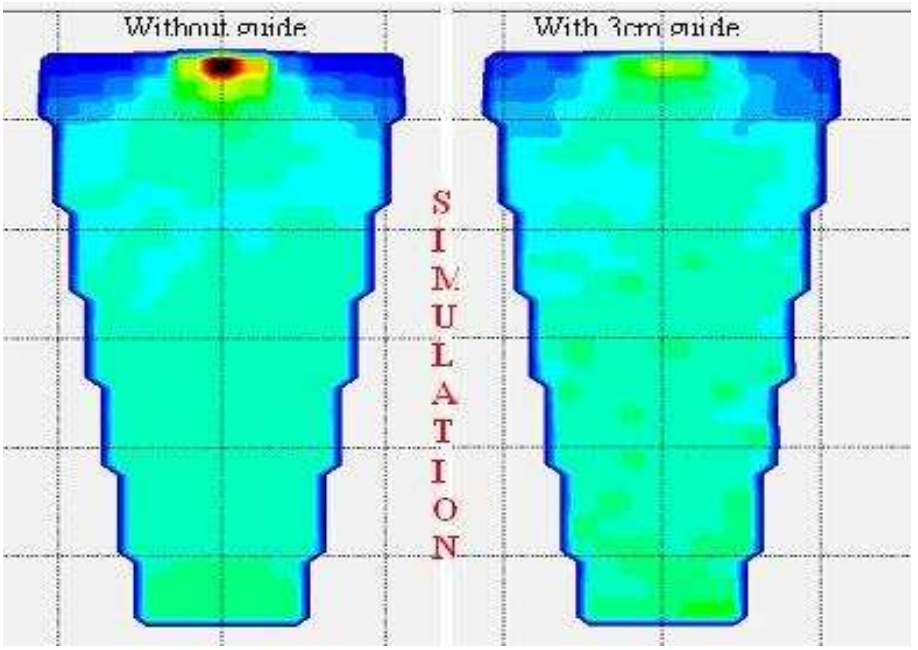

Figure 13. The simulated light guide effect, assuming a configuration with aluminum wrapping, optical gel, and a 2+1 light guide.

5.3 Blind regions

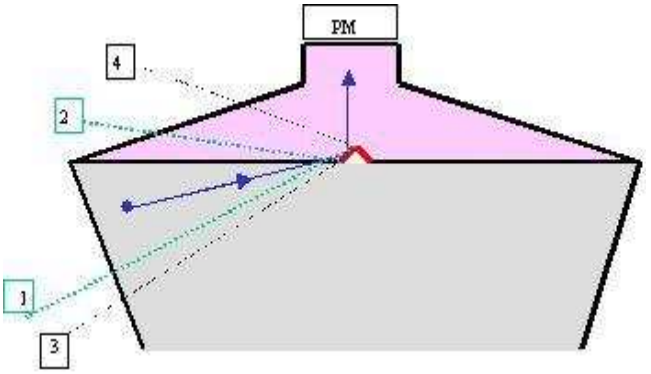

Figure 14. The triangular cut advantages: all photons issued from the region delimitated by straight lines 1 and 2 and which arrive at the reflective surface of the triangular cut, go directly towards the PMT entrance.

While the light collection uniformity is improved with a light guide, there is still a low amplitude region corresponding to the corners. It was then proposed to make a triangular cut in the light guide to reflect the light originating from these regions.

As shown on Fig. 14, the proposed triangular cut, wich is wrapped with aluminium, acts as a mirror. It provides an obstacle for the direct view of the PMT while reflecting photons from the corner regions. This reduces the difference between extreme amplitudes and consequently improves the light collection uniformity.

Tr. Cut	$\mathbf{\Delta A}$	$\delta\Delta\mathbf{A}$	$\mathbf{A}_{\mathbf{M}in}$	$\mathbf{A}_{\mathbf{M}ax}$
(0.125 - 0.250)	0.301	0.02	0.812	1.112
(0.125 - 0.500)	0.333	0.02	0.785	1.118
(0.125 - 1.000)	0.499	0.02	0.701	1.201
(0.250 - 0.250)	0.295	0.02	0.825	1.120
(0.250 - 0.500)	0.329	0.02	0.782	1.111
(0.250 - 1.000)	0.324	0.02	0.800	1.124
(0.500 - 0.125)	0.266	0.02	0.838	1.104
(0.500 - 0.200)	0.194	0.02	0.885	1.079
(0.500 - 0.250)	0.200	0.02	0.894	1.095
(0.500 - 0.300)	0.249	0.02	0.900	1.149
(0.500 - 0.500)	0.269	0.02	0.812	1.081
(0.500 - 1.000)	0.378	0.02	0.787	1.165
(1.000 - 0.250)	0.323	0.02	0.742	1.066
(1.000 - 0.500)	0.469	0.02	0.763	1.231
(1.000 - 1.000)	0.603	0.02	0.788	1.391
(2.000 - 0.250)	0.537	0.02	0.702	1.239
(2.000 - 0.500)	0.442	0.02	0.740	1.182
(2.000 - 1.000)	0.795	0.02	0.690	1.484

Table 2. Optimization of the triangular cut: in the *Tr. Cut* column, the 1^{st} number gives the triangle base and the 2^{nd} one represents its height.

Simulation were performed in order to optimize the base and the height of the triangular cut. Results, reported in Tab. 2, gives the best uniformity for a 5 mm base and 2 mm height. The configuration (5 - 2.5) was finally selected for an easy and cheap machining, introducing, according to simulations, a negligible effect on the light collection uniformity.
This new configuration has been experimentally tested using the two prototype paddles: paddle A with a simple light guide and paddle B with a triangular cut. The experimental light collection maps are compared on Fig. 15. First,

it is observed that the use of a light guide improves the amplitude in the corner regions and reduces the amplitude in front of the PMT, leading to a 53% improvement of the light collection uniformity as compared to a paddle without guide. Second, the triangular cut (Fig. 16) reduces the magnitude of the high amplitude region in front of the PMT and minimizes the corner regions where amplitudes are below average. As compared to a simple guide, a 22% improvement of the light collection uniformity is obtained. In addition, these modifications of the original prototype configuration do not affect the signal shape and width.

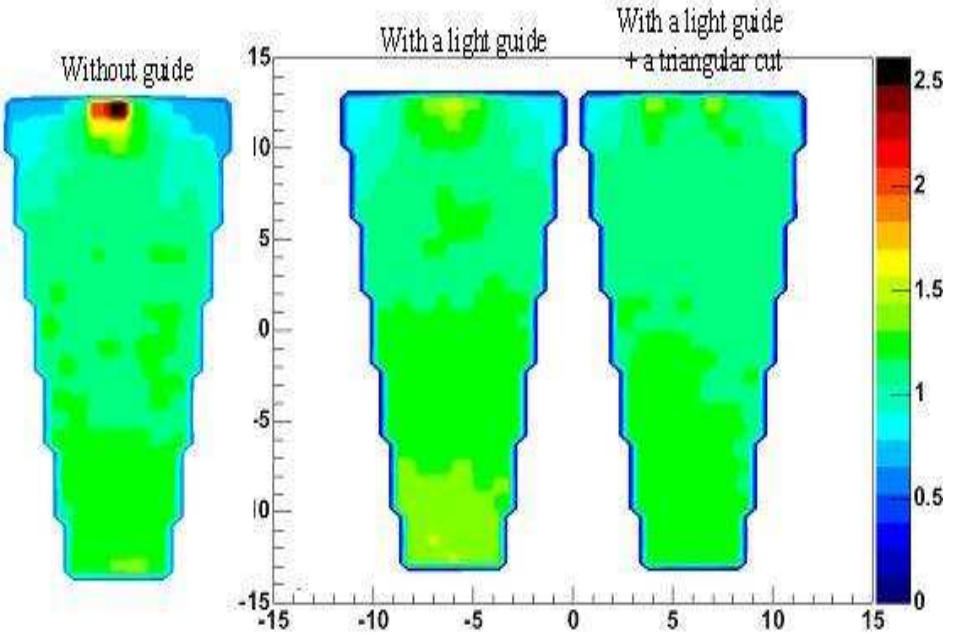

Figure 15. Comparison of the experimental light collection map for the different configurations.

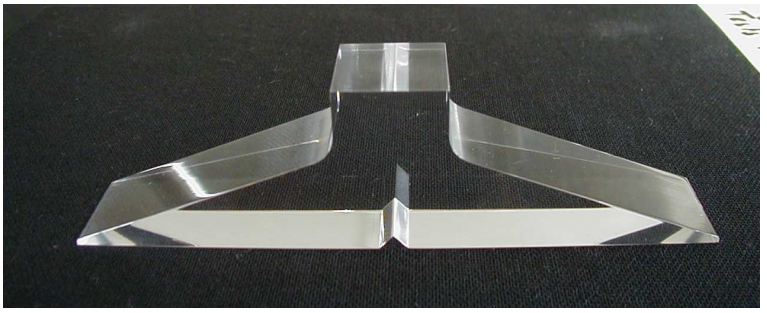

Figure 16. The triangular cut of the light guide.

6 Conclusions

Using a light guide with a triangular cut, the variation of the signal amplitude due to the origin of the emitted light is only about 33%, as comparison to

150% for the initial prototype configuration. Therefore, all paddles of the DVCS tagger will be wrapped with aluminum wrapping and a 3 cm high light guide. Nevertheless, the triangular cut will equip only the light guides of the full size paddles, the corner effects being much reduced for half size paddles. The final scintillators are smaller than the prototype paddles (within about 1 cm), and the straight part of the light guide has been reduced to 4 mm. These should all combine into a better light collection uniformity for the actual detector.

References

[1] Jefferson Lab Experiment **E03-106**, P. Bertin, C. Hyde-Wright, F. Sabatié, E. Voutier, spokespeople;
http://hallaweb.jlab.org/experiment/DVCS.

[2] N. Baier, Diploma Dissertation, Ecole Nationale Supérieure de Physique, Strasbourg (France), 2003;
http://hallaweb.jlab.org/experiment/DVCS/docs.html.

[3] NES Technology S.A., 2 rue De-Grenus, 1201 Genève, Switzerland;
http://www.wnes.net

[4] http://gentit.home.cern.ch/gentit/litrani/

ANNEX: Simulation results

The following tables list the different configurations and their corresponding simulation results. The light collection map, referenced by the page number in column 1, can be found at
http://www.jlab.org/~mazouz/simu.

The third number in guide column means that the guide starts with a straight part.

Pg.	Paddle	Wrap.	Gel	Guide	Nature	ΔA	A_{Min}	A_{Max}
1	full	Alu.	N	None		0.93	0.56	1.49
2	full	Alu.	Y	None		1.25	0.61	1.86
3	full	Alu.	N	2+0	PMMA	0.72	0.57	1.29
4	full	Alu.	Y	2+0	PMMA	0.33	0.82	1.15
5	full	Alu.	N	2+1	PMMA	0.75	0.55	1.30
6	full	Alu.	Y	2+1	PMMA	0.35	0.78	1.13
7	full	Mil.	N	None		0.64	0.68	1.32
8	full	Mil.	Y	None		0.80	0.79	1.59
9	full	Mil.	N	2+0	PMMA	0.56	0.69	1.25
10	full	Mil.	Y	2+0	PMMA	0.28	0.81	1.09
11	full	Mil.	N	2+1	PMMA	0.55	0.69	1.24
12	full	Mil.	Y	2+1	PMMA	0.25	0.85	1.10
13	full	Alu.	Y	1+0	SCINT	0.56	0.72	1.28
14	full	Alu.	Y	2+0	SCINT	0.42	0.77	1.19
15	full	Alu.	Y	1+1	SCINT	1.18	0.55	1.73
16	full	Alu.	Y	2+1	SCINT	0.72	0.7	1.42
17	full	Mil.	Y	1+0	SCINT	0.45	0.69	1.14
18	full	Mil.	Y	2+0	SCINT	0.36	0.78	1.14
19	full	Mil.	Y	1+1	SCINT	0.50	0.68	1.18
20	full	Mil.	Y	2+1	SCINT	0.32	0.77	1.09
21	half 1	Alu.	N	None		0.49	0.76	1.25

...

...

22	half 1	Alu.	Y	None		0.54	0.7	1.24
23	half 1	Alu.	Y	2+0	PMMA	0.27	0.85	1.12
24	half 1	Alu.	Y	2+1	PMMA	0.30	0.83	1.13
25	half 1	Mil.	Y	2+0	PMMA	0.17	0.91	1.08
26	half 1	Mil.	Y	2+1	PMMA	0.17	0.92	1.09
27	half 1	Mil.	N	None		0.62	0.71	1.33
28	half 1	Mil.	Y	None		0.4	0.72	1.12
29	half 1	Alu.	Y	2+0	SCINT	0.20	0.9	1.10
30	half 1	Alu.	Y	2+1	SCINT	0.08	0.93	1.01
31	half 1	Mil.	Y	2+0	SCINT	0.1	0.94	1.04
32	half 1	Mil.	Y	2+1	SCINT	0.13	0.94	1.07
33	half 2	Alu.	N	None		0.89	0.55	1.44
34	half 2	Alu.	Y	None		0.74	0.62	1.36
35	half 2	Alu.	Y	2+0	PMMA	0.37	0.81	1.18
36	half 2	Alu.	Y	2+1	PMMA	0.51	0.78	1.29
37	half 2	Mil.	Y	2+0	PMMA	0.30	0.82	1.12
38	half 2	Mil.	Y	2+1	PMMA	0.28	0.84	1.12
39	half 2	Mil.	N	None		1.13	0.54	1.67
40	half 2	Mil.	Y	None		0.40	0.73	1.13
41	half 2	Alu.	Y	2+0	SCINT	0.37	0.86	1.23
42	half 2	Alu.	Y	2+1	SCINT	0.34	0.85	1.19
43	half 2	Mil.	Y	2+0	SCINT	0.24	0.91	1.15
44	half 2	Mil.	Y	2+1	SCINT	0.18	0.91	1.09
45	full	Alu.	N	2+0	PMMA	0.56	0.70	1.26
46	full	Mil.	N	2+0	PMMA	0.38	0.80	1.18
47	full	Alu.	Y	2+1	PMMA	0.39	0.79	1.18
48	full	Alu.	Y	1+1+1	PMMA	0.46	0.71	1.17
49	full	Alu.	Y	3+1	PMMA	0.39	0.81	1.20
50	full	Alu.	Y	1.5+1.5+1	PMMA	0.38	0.79	1.17

...

...

51	full	Mil.	Y	2+1	PMMA	0.25	0.86	1.11
52	full	Mil.	Y	1+1+1	PMMA	0.26	0.86	1.12
53	full	Mil.	Y	3+1	PMMA	0.22	0.88	1.10
54	full	Mil.	Y	1.5+1.5+1	PMMA	0.24	0.87	1.11
55	full	Alu.	Y	3+1	PMMA	0.89	0.55	1.44
56	full	Alu.	Y	3+0	PMMA	0.74	0.62	1.36
Pg.	**Paddle**	**Wrap.**	**Gel**	**Guide**	**Nature**	**ΔA**	**A_{Min}**	**A_{Max}**

Pg.	**Tr. Cut**	**ΔA**	**A_{Min}**	**A_{Max}**
57	2+1 (0.250 - 0.250)	0.301	0.812	1.112
58	2+1 (0.250 - 0.500)	0.333	0.785	1.118
59	2+1 (0.250 - 1.000)	0.499	0.701	1.201
60	2+1 (0.500 - 0.250)	0.295	0.825	1.120
61	2+1 (0.500 - 0.500)	0.329	0.782	1.111
62	2+1 (0.500 - 1.000)	0.324	0.800	1.124
63	2+1 (1.000 - 0.125)	0.266	0.838	1.104
64	2+1 (1.000 - 0.200)	0.194	0.885	1.079
65	2+1 (1.000 - 0.250)	0.200	0.894	1.095
66	2+1 (1.000 - 0.250)	0.273	0.875	1.148
67	2+1 (1.000 - 0.300)	0.249	0.900	1.149
68	2+1 (1.000 - 0.500)	0.269	0.812	1.081
69	2+1 (1.000 - 1.000)	0.378	0.787	1.165
70	2+1 (2.000 - 0.250)	0.323	0.742	1.066
71	2+1 (2.000 - 0.500)	0.469	0.763	1.231
72	2+1 (2.000 - 1.000)	0.603	0.788	1.391
73	2+1 (4.000 - 0.250)	0.537	0.702	1.239
74	2+1 (4.000 - 0.500)	0.442	0.740	1.182
75	2+1 (4.000 - 1.000)	0.795	0.690	1.484